文章编号:1001 - 9014(2011)03 - 0193 - 04

Performance of the continuous-wave imaging system based on a terahertz gas laser

WANG Ying-Xin[1,2], ZHAO Zi-Ran[2], CHEN Zhi-Qiang[2],
ZHANG Li[2], KANG Ke-Jun[2], DENG Jing-Kang[1]
(1. Department of Physics, Tsinghua University, Beijing 100084, China;
2. Department of Engineering Physics, Tsinghua University, Key Laboratory of Particle & Radiation Imaging, Ministry of Education, Beijing 100084, China)

Abstract: Continuous-wave terahertz imaging was demonstrated based on an optically-pumped far-infrared gas laser and a Golay cell detector. The imaging system design and construction are discussed in the context of the choice and configuration of the involved terahertz optical components and devices. Performance characteristics of the system, including signal-to-noise ratio, spatial resolution, detector response and imaging speed were measured and analyzed in detail. With this system, terahertz transmission images of various samples were obtained, confirming the quality of our setup and supporting the feasibility of terahertz imaging technique for applications in security screening and quality control. A data processing method for automatic calibration of the image intensities in the background region was also proposed to remove the influence of laser power drift on the image quality.

Key words: terahertz; continuous wave; imaging system; far-infrared laser
PACS: 42.30.Va, 42.62.Cf

基于太赫兹气体激光器的连续波成像系统性能分析

王迎新[1,2], 赵自然[2], 陈志强[2], 张 丽[2], 康克军[2], 邓景康[1]
(1. 清华大学 物理系, 北京 100084;
2. 清华大学 工程物理系 粒子技术与辐射成像教育部重点实验室, 北京 100084)

摘要: 实现了基于光泵浦远红外气体激光器和高莱管探测器的连续波太赫兹成像. 从太赫兹光学器件的选择和配置角度讨论了成像系统的设计和搭建流程. 详细测试了系统在信噪比、空间分辨率、探测器响应和成像速度方面的性能指标. 利用该系统采集了一系列样品的太赫兹透射图像,实验结果验证了系统的成像效果,揭示出太赫兹成像技术在安全检查和质量控制方面的应用可行性. 为了消除激光器功率漂移对图像质量的影响,提出了一种对图像背景区强度进行自动校准的数据处理方法.

关 键 词: 太赫兹; 连续波; 成像系统; 远红外激光器
中图分类号: O439 **文献标识码**: A

Introduction

Terahertz radiation, lying between the millimeter waves and infrared (0.1 ~ 10THz), has good penetrability to most nonmetallic and non-polar materials. This ability makes terahertz radiation an effective and complementary imaging source for revealing the structure information of the object. Since the first demonstration of pulsed terahertz imaging system by Hu and Nuss[1], many investigations have been conducted to explore the applications of terahertz imaging in various fields, such as biomedical diagnostics[2], security screening[3],

Received date: 2010 - 04 - 08, **revised date**: 2011 - 03 - 05 **收稿日期**:2010 - 04 - 08, **修回日期**:2011 - 03 - 05
Foudantion item: Supported by China Postdoctoral Foundation(20100470017)
Biography: WANG Ying-Xin (1981-), male, Liaoning, China, Research Assistant. Research area is terahertz spectroscopy and imaging. E-mail: wangyingxin2000@tsinghua.org.cn.

and quality control[4]. The imaging modalities can be divided into two categories: pulsed (or time-domain) imaging and continuous-wave (CW) imaging.

Pulsed terahertz system is able to provide rich information about the object both in the time and frequency domain. However, the pump-probe measurement configuration produces a large increase in system complexity[5]. Real-time two-dimensional (2D) pulsed imaging could be achieved by a large-area (cm^2) electro-optic crystal sensor[6], but the energy density decrease of the expanded beam will reduce the signal-to-noise ratio (SNR). On the other hand, terahertz radiation undergoes strong atmospheric attenuation at certain frequencies (>10dB/m around the water vapor absorption lines[7]) for standoff detection applications. In this situation, narrow-band (or CW) terahertz generators are more suitable. Recently, many kinds of CW systems based on different sources have been reported[5,7~10]. Compared to pulsed system, the CW system generally exhibits advantages of high average power, simple alignment, compactness and relatively low cost.

To perform theoretical and applied research on terahertz imaging technique, we have built up an experimental system consisting of a CW source and a direct detector. In this paper we present a detailed description of our imaging setup from the viewpoints of design, construction, characterization and operation. Some preliminary experimental results are included to demonstrate the system performance.

1 Imaging setup

Taking into account the factors of output power, beam quality and operation temperature, an optically-pumped FIR laser (OPFIRL) is employed for terahertz generation. For detection a Golay cell is appropriate due to its relatively high sensitivity and room temperature operation.

Fig. 1 (a) illustrates the optical layout of our imaging system. The OPFIRL (FIRL 100, Edinburgh Instruments Ltd., UK) generates monochromatic FIR radiation emitted from gaseous organic molecules that are pumped by a grating-tuned CO_2 laser. Table I lists the FIR data of five prominent pump lines with methanol (CH_3OH) as the lasant, where the most powerful one, i.e., the 9P36 line, was utilized.

Two gold-coated mirrors M1 and M2 were used to guide terahertz waves to the sample region. For an air environment with a relative humidity of 40%, the atmospheric absorption coefficient is 0.16 m^{-1} at 2.52 THz[12]. Thus the power loss is 1.26 dB (attenuated to about 75%) after a propagation distance of 1.8 m. This value would serve as a reference for setting the source-to-detector distance in system design. We chose high-density polyethylene (HDPE) lenses to focus and collimate the terahertz beam since HDPE is highly transparent at this frequency range (absorption coefficient $\alpha = 0.75$ cm^{-1} at 2.52 THz[11]). All lenses have a clear aperture of 50 mm. The focal lengths of L1, L2, and L3 are 60, 60, and 120 mm, respectively.

Detection was achieved with a Golay cell. It can operate with a typical noise equivalent power (NEP) of about 10 $nW/Hz^{1/2}$ and a responsivity exceeding 10 kV/W at 12.5 Hz modulation. To avoid detector saturation, an attenuator set with four transmission levels was inserted at the FIR beam exit. In addition, an optical chopper was introduced to create a modulated radiation input for the Golay cell. The data collection and processing system consisted of a lock-in amplifier (LIA) and a control computer. The sample was mounted on a pair of mechanical translation stages and the image was acquired by moving the stages point by point. The photograph of our experimental setup is shown in Fig. 1(b).

2 System performance analysis

2.1 Signal-to-noise ratio

Sources of noise in our system mainly come from two aspects: thermal background radiation and FIR laser power fluctuation. The background noise level corresponds to the variation of the amplitude of the detector's output signal in the absence of terahertz beam illumination. This level was observed to be approximately $U_n = 5$ mV. The maximum signal magnitude of Golay cell is $U_S = 3$ V, thus, the SNR is equal to $U_S/U_n = 600$ when considering only the thermal background. In order to analyze the laser fluctuation, the radiation intensity was measured as a function of operating time.

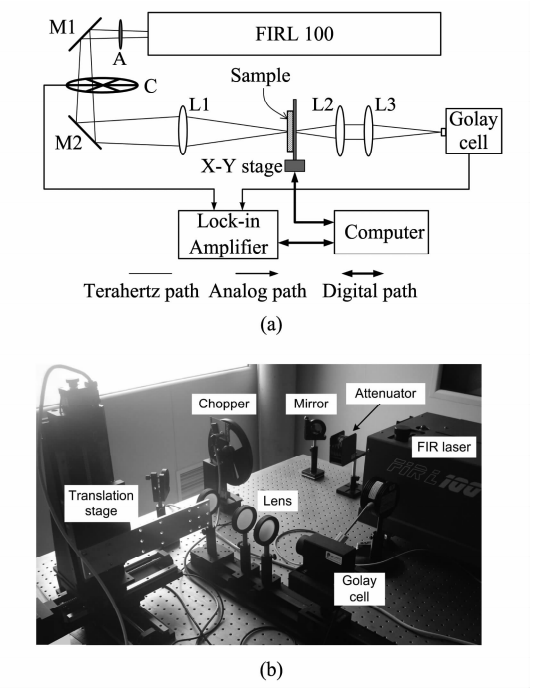

Fig. 1　(a) Schematic diagram of the continuous-wave terahertz imaging setup. A, attenuator; C, chopper; M1, M2, mirrors; L1-L3, lenses (b) Photograph of the imaging setup
图 1　(a)连续波成像实验系统结构示意图. A, 衰减器; C, 斩波器; M1,M2, 反射镜; L1-I4, 透镜 (b)成像系统照片

The data was recorded every 10 sec over a total time of 20min. Fig. 2 shows the power fluctuation curve, where the fast oscillations are due to the long measurement interval. Linear fit of the curve implies a gradual decrease in power level, meaning that a short measurement time in the imaging experiment would be preferable. The mean value and standard deviation of the power are $P_m = 81.2$ mW and $P_d = 1.7$ mW respectively, yielding a SNR of $P_m/P_d = 47.8$ (i. e., 34 dB). This indicates that the laser fluctuation is a dominated noise source and therefore ensuring the laser power stability acts as a key factor to improve the SNR.

Table 1　Transition parameters of CH_3OH pumped by five different CO_2 lines
表 1　五种 CO_2 谱线泵浦下甲醇分子的跃迁参数

CO_2 line	9P34	9R8	9R10	9P36	10R38
Wavelenth(μm)	70.6	86.2	96.5	118.8	163
Frequency(THz)	4.25	3.48	3.11	2.52	1.84
Typical power level(mW)	20	10	90	150	36

2.2　Spatial resolution

The spatial resolution of the imaging system is determined by the FIR beam spot size at the sample plane. We used the knife-edge method to evaluate it. A metallic blade was placed at the beam focus and scanned along the x and y directions perpendicular to the orientation of its edge, with a step size of 0.05 mm. The solid lines in Fig. 3 represent the transmission intensity of terahertz radiation versus the knife edge position. Assuming Gaussian transverse intensity profile for the FIR beam, the transmission signal can be expressed as

$$I(x) = \frac{I_0}{2}\left[1 + \frac{2}{\sqrt{\pi}}\int_0^{x/w} \exp(-t^2)\,\mathrm{d}t\right], \quad (1)$$

where I_0 is the full beam intensity, x is the knife edge position (offset from the beam center), and w is the half-width at $1/e$ of the distribution. We calculated the derivative of the measured $I(x)$ and then fit it to a Gaussian function. The results are also shown in Fig. 3. The spot sizes (w) in x and y directions were obtained to be 0.73 and 0.56 mm, respectively, which reflects that the measured focal spot has a somewhat elliptical shape, possibly owing to the error in scanning direction. According to these parameters, we conclude that the spatial resolution (equivalent to diameter at half-height, $2\sqrt{\ln 2}w$) of our system is approximately 1 mm.

If we suppose the beam waist is $\bar{w} = 0.6$ mm, the depth of focus (DOF, defined as twice the Rayleigh range of the focused beam) is readily computed to be 19 mm. This parameter determines the tolerant thickness and axial position of the imaged sample. There is a tradeoff between the spatial resolution and the DOF. A focusing system with a smaller focal spot size leads to a higher resolution but a shorter DOF.

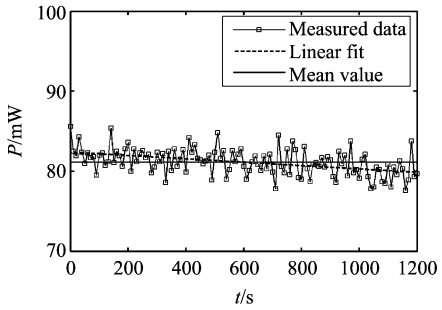

Fig. 2　Stability test for the laser output power
图 2　激光器输出功率的稳定性测试

2.3　Detector response

In order to test the linearity of the detector

response, we measured the detector output signal for different incident power. Modulation of the terahertz radiation power level was made by an attenuator. By choosing three transmission levels of the attenuator (3%, 10%, and 30%), together with the full transmission case, four different incident intensities could be obtained. The output waveforms of the Golay cell were recorded, as shown in Fig. 4(a). Fig. 4(b) shows the relation between the average signal intensity and the transmission level. A linear fit to the data points gives a correlation coefficient of 0.99997 and a small intercept, which verifies that the Golay cell detector has a good linear response.

2.4 Imaging speed

The imaging speed depends on the time needed for measuring one pixel and the scanning speed of the translation stage. Although Golay cell is a sensitive detector, it has a long response time (several tens of ms), limiting the chopper frequency and the LIA time constant. Our experiments were performed at a time constant of 300 ms; thus one second dwell time is generally required for each pixel. A smaller time constant allows a rapider data acquisition, whereas the SNR will degrade. The translation stage has a maximal motion speed of 20 mm/s, and imaging rate of 40 pixels/s would be expected at 0.5-mm step size without accounting for the detector response. Consequently, the imaging speed of our system is limited by the measurement time for each pixel.

3 Imaging examples

In what follows we present several preliminary experimental results to assess the imaging capability of our system as well as illustrate the potential applications of terahertz imaging.

The first sample is a razor blade concealed in a regular paper envelope, as shown in Fig. 5(a). It was scanned with a 0.5-mm step size over the area indicated by the dashed square (27×27 mm^2). The LIA was referenced to a chopper frequency of 25 Hz and the integration time was set to be 300 ms. Under these conditions, the image acquisition time was about 70 min. Fig. 5(b) shows the resulting image mapped by terahertz transmission intensity. We can see that the blade is clearly resolved. However, variation in background intensity along the vertical direction reflects a

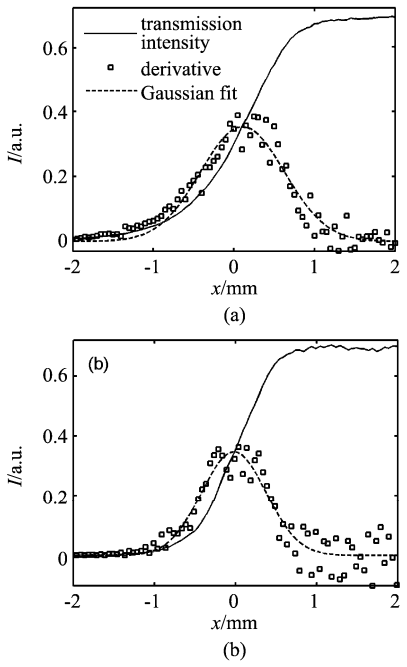

Fig. 3 FIR beam spot size measurement at the sample plane. Panels (a) and (b) are for x and y directions, respectively
图3 样品平面FIR光斑尺寸测量.(a)和(b)分别代表x和y方向

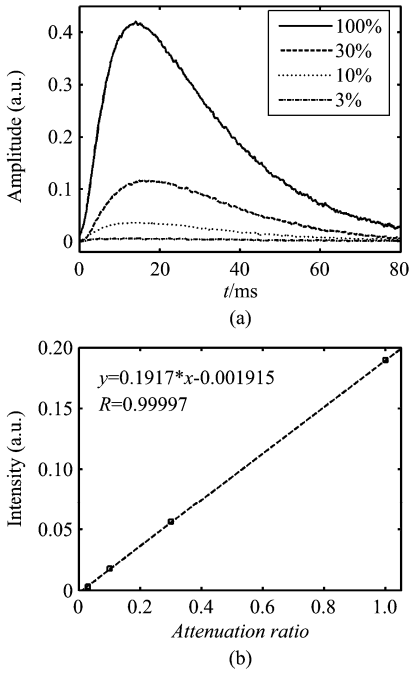

Fig. 4 (a) Output signal of the detector with different input power (b) Signal intensity as a function of the attenuator ratio
图4 (a)不同入射功率下探测器输出信号波形 (b)信号强度与衰减率的关系

fact that the terahertz signal decreases gradually, which arises from FIR laser power drift (see Fig. 2). To solve this problem, we introduce a calibration method. Following the discussion in Section 2.1, the terahertz signal decrease can be approximated to have a linear relation with the measurement time, i.e., $I(t) = At + I(0)$. A and $I(0)$ are determined by linear fitting of the pixel values in the background region. Thus, for any pixel measured at a known time, we have a reference intensity. Dividing the raw image by these reference values yields a calibrated image, i.e.,

$$I_{\mathrm{cal}}(i,j) = \frac{I_{\mathrm{raw}}(i,j)}{At(i,j) + I(0)} \quad , \qquad (2)$$

where (i,j) denotes the pixel index. Fig. 5(c) displays the image after calibration. It is obvious that the background region becomes more uniform, verifying the effectiveness of our calibration method. This imaging example demonstrates that terahertz radiation is capable to see through some visually opaque materials and detect concealed objects. Hence, terahertz imaging reveals a potential application in security screening.

The feasibility of CW terahertz imaging applied for nondestructive quality control was evaluated through another two examples. One is a paper envelope inside of which the letters "THU" are written with a pencil, as shown in Fig. 6(a). The scanning area and step size are 34×15 mm^2 and 0.5 mm, respectively. Fig. 6(b) shows the corresponding terahertz image with background calibration. Due to the appropriate penetration capability of terahertz radiation, these letters are visualized with good contrast. This experiment illustrates the possible use of terahertz imaging in the field of artwork inspection. Fig. 6(c) and 6(d) show the other example, the plastic cover of a USB flash drive. Although plastic is nearly transparent to terahertz waves, all the edge features on the sample are highlighted because of the existence of scattering or diffraction effect. Such properties enable nondestructive material testing using this imaging technique. The fringe patterns in the lower part of Fig. 6(d) are the result of standing wave effect caused by reflections from the system and the sample.

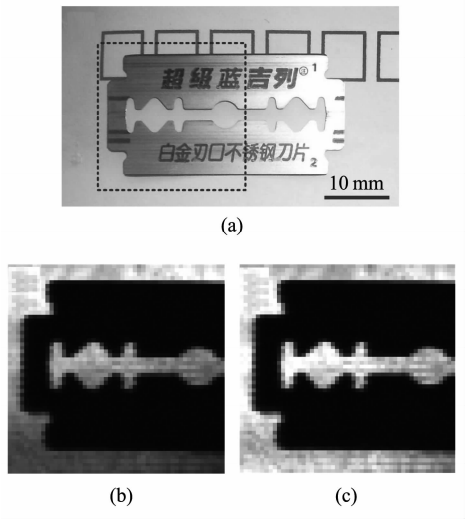

Fig. 5　Imaging results of a blade wrapped in an envelope (a) Photograph of the sample (b) Raw image (c) Processed image with background calibration

图 5　信封中隐藏刀片的成像结果 (a)样品照片 (b)原始图像 (c)经过校准的图像

4　Conclusion

We have developed a CW imaging system using an OPFIRL as the terahertz radiation source and a Golay cell as the detector. The system noise is induced primarily by the power fluctuation of the FIR laser. The SNR was estimated to be 34 dB for 20-min monitoring time. Experimental measurement on the beam spot size at the sample plane showed that our system had a spatial resolution of about 1 mm. Within the dynamic range of the detector, an ideal linear response was observed. Limited by the acquisition time for each pixel,

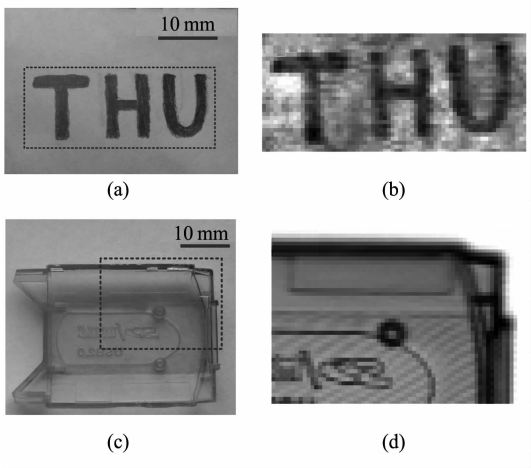

Fig. 6　Imaging results of pencil letters written on inside of an envelope (a,b) and a plastic sample (c,d)

图 6　信封内铅笔字迹(a,b)和塑料样品(c,d)成像结果

(下转 236 页)

str. Meth A,2002,**494**:308—312.
[2] Lecoq P. Ten years of lead tungstate development[J]. *Instr. Meth A: Accelerators, Spectrometers, Detectors and Associated Equipment*,2005,**537**(1~2):15—21 .
[3] SHAO Jun, MA Li-Li, LU Xiang, *et al*, RECENT PROGRESS AND POTENTIAL IMPACT OF MODULATION SPECTROSCOPY FOR NARROW-GAP HgCdTe[J]. *J. Infrared Millim. Waves*(邵军,马丽丽,吕翔,等. 窄禁带碲镉汞调制光谱的近期研究进展和前景. **红外与毫米波学报**),2008,**27**(2):1—6.
[4] WAN You-Bao, WU Ru-Rong, ZHANG Jian-Xin, *et al*. The Influence of Ions Doped Concentration on the Scintillation Optical properties of BaF_2:$PbWO_4$ Crystals[J]. *J. Infrared Millim. Waves*(万尤宝, 吴宇容,张建新,等. 掺杂钨酸铅闪烁晶体的闪烁光学性质研究. **红外与毫米波学报**),2009,**28**(4):263—266.
[5] SHAN Xia-guisi, The Application of PWO on PET[C]. *Proceeding on Bilateral Symposium Digest for Phonic Science and Industry*, Hangzhou, China, 2000, 20—25.
[6] YANG Peizhi., Growth of large-size crystal of PbWO4 by vertical Bridgman method with multi-crucibles [J]. *J. Cryst. Growth*,2002,**236**(4):589—595.
[7] WAN youbao, The multi-crucible system for crystal growth [P]. CN 200610148319.4, (万尤宝,多坩埚温梯法晶体生长系统,CN 200610148319.4)
[8] Moreau J M, Structural characterization of $PbWO_4$ and related new phase $Pb_7W_8O_{32}$-x [J]. *J. All. and Comp.*,1996, **238**:46—48.
[9] Williams R T, Zhang Y C, Abraham Y, *et al*, The Spectrum Character of PWO crystal[J]. *Proceedings on ICISA*^{15th},2000,**118**.
[10] Ye Chongzhi, Liao Jingying, *et al*. Growth and scintillation properties of F doped $PbWO_4$ crystals[J]. *Nucl. Instr. Meth. A*. 2006,**566**:757.

(上接 197 页)

the imaging speed was on the order of one pixel per second. Imaging examples of concealed metallic object and transparent dielectric materials have demonstrated the performance of our system and potential applications of terahertz imaging. Further improvements in terms of SNR and imaging speed are necessary. Synchronously recording the output power of the FIR laser with another detector to offer a reference signal may solve the problem of laser fluctuation and reduce the noise. Continuously scanning the sample in one dimension or replace the translation stage by a galvanometer could shorten the imaging time. These strategies will be considered in future work.

REFERENCES

[1] Hu B B, Nuss M C. Imaging with terahertz waves [J]. *Opt. Lett.*,1995,20(16):1716—1718.
[2] Taylor Z D, Singh R S, Culjat M O, *et al*. Reflective terahertz imaging of porcine skin burns[J]. *Opt. Lett.*,2008, **33**(11):1258—1260.
[3] Federici J F, Schulkin B, Huang F, *et al*. THz imaging and sensing for security applications—explosives, weapons and drugs[J]. *Semicond. Sci. Technol.*,2005,**20**(7):S266—S280.
[4] Jördens C, Koch M. Detection of foreign bodies in chocolate with pulsed terahertz spectroscopy[J]. *Opt. Eng.*,2008,**47**(3):037003.
[5] Karpowicz N, Zhong H, Xu J, *et al*. Comparison between pulsed terahertz time-domain imaging and continuous wave terahertz imaging [J]. *Semicond. Sci. Technol.*,2005,**20**(7):S293—S299.
[6] Chan W L, Deibel J, Mittleman D M. Imaging with terahertz radiation [J]. *Rep. Prog. Phys.*, 2007, **70**(8): 1325—1379.
[7] Lee A W M, Qin Q, Kumar S, *et al*. Real-time terahertz imaging over a standoff distance (>25meters)[J]. *Appl. Phys. Lett.*,2006,**89**(14): 141125.
[8] Kawase K, Ogawa Y, Watanabe Y. Non-destructive terahertz imaging of illicit drugs using spectral fingerprints[J]. *Opt. Express*,2003,**11**(20):2549—2554.
[9] Ge X H, Lü M, Zhong H, *et al*. Terahertz wave reflection imaging system based on backward wave oscillator and its application[J]. *J. of Infrared Millim. Waves*(葛新浩,吕默,钟华,等. 反射式太赫兹返波振荡器成像系统及其应用. **红外与毫米波学报**),2010,**29**(1):15—18.
[10] Yang J, Ruan S, Zhang M. Real-time, continuous-wave terahertz imaging by a pyroelectric camera[J]. *Chin. Opt. Lett.*,2008,**6**(1):29—31.
[11] Lee Y S. Principles of terahertz science and technology [M]. New York: Springer, 2009.
[12] Linden K J, Neal W R, Waldman J, *et al*. Terahertz laser based standoff imaging system: proceedings of the 34th Applied Imagery Recognition Workshop, 2005[C]. Washington, D. C.: IEEE Computer Society, 2005.